Korean J. Chem. Eng., 32(11), 2335-2341 (2015)
DOI: 10.1007/s11814-015-0070-6

pISSN: 0256-1115
eISSN: 1975-7220

Novel perpendicularly cross-rectangular CuO architectures: Controlled synthesis, enhanced photocatalytic activity and catalytic thermal-decomposition of NH_4ClO_4

Hanmei Hu*,,†, Xinqing Ge*, Qiang Zheng*, and Chonghai Deng***,†**

*Key Laboratory of Functional molecule Design and Interface Process, Anhui University of Architecture, Hefei 230601, China
**School of Materials and Chemical Engineering, Anhui University of Architecture, Hefei 230601, China
***Department of Chemical and Materials Engineering, Hefei University, Hefei 230601, China
(*Received 12 September 2014 • accepted 7 April 2015*)

Abstract−Novel perpendicularly cross-rectangular CuO architectures have been successfully fabricated on a large scale by a facile microwave-assisted chemical aqueous route. The as-synthesized CuO products were characterized by X-ray diffraction (XRD), field emission scanning electron microscopy (FESEM), transmission electron microscopy (TEM), selected area electron diffraction (SAED), high resolution transmission electron microscopy (HRTEM) and UV-vis absorption spectroscopy. An individual CuO microstructure is mainly assembled by two rectangle-shaped nanosheets with different sizes, which is perpendicularly intersected through the center. A possible formation mechanism of perpendicularly cross-rectangular CuO architectures was proposed based on the comparative experimental results. The prepared CuO nanoarchitectures exhibited excellent photocatalytic activity for the decolorization of Rhodamine B (RhB) under visible light irradiation. Simultaneously, the prepared CuO products, acting as an additive, also showed effective catalytic activity on the thermal decomposition of ammonium perchlorate (NH_4ClO_4).

Keywords: Crystal Growth, CuO Nanosheets, Green Synthesis, Catalytic Performance

INTRODUCTION

Metal oxide nanostructured materials with uniform shape and size have attracted considerable attention due to their importance in scientific research and potential applications in the future [1-5]. Cupric oxide (CuO), an important p-type transition-metal semiconductor, has received much attention due to its potential applications in various regions, such as gas sensing [6], catalysts [7], magnetic storage media [8], superconductors [9], lithium ion electrode materials [10] and field-emission (FE) emitters [11].

Based on the fundamental and practical importance of CuO nanomaterials, many efforts have been directed toward the preparation of CuO with special morphology to enhance its performance in currently existing applications. So, a variety of simple and complex structures of CuO have been reported in the literature, such as nanoparticles [12], nanorods [13], nanowires [14], nanobelts [15], nanorings [16], nanotablets [17], nanoboxes [18], spindly nanocrystals [19], dendrite-shaped CuO hollow micro/nanostructures [20], nanoplatelets with well-aligned arrays [21], rose-like nanoarchitectures [22], urchin-like microcrystals [23], perpendicularly cross-bedded microstructures [24], microscale cog-like superstructures [25], well-defined cauliflowers [26], and so on. However, experimental trials and growth mechanism studies for CuO special micro/nanostructures are inadequate. The controlled synthesis of CuO highly regular patterns and their potential applications are still challenging in chemistry and materials science.

We have developed a facile microwave-assisted chemical synthetic route to fabricate novel perpendicularly cross-rectangular CuO architectures on a large scale. The synthetic method is simple and environment-friendly, which does not need high reaction temperature and long reaction time. Such a perpendicularly cross-rectangular architecture has rarely been reported in the literature. The influencing factors and growth mechanism of perpendicularly cross-rectangular CuO architectures in the solution were clarified. The photocatalytic performance of as-prepared CuO cross-rectangular architectures was studied by degrading Rhodamine B (RhB) in water under visible light irradiation. And the catalytic property of the CuO nanoarchitectures on the thermal decomposition of ammonium perchlorate (NH_4ClO_4) was also investigated. By comparing as-prepared CuO with commercial CuO, a conclusion can be drawn that as-prepared CuO cross-rectangular architectures have more stronger ability to quickly photocatalytic degradation of organic dyes and have more effective catalytic activity on the thermal decomposition of ammonium perchlorate. We think the main reason is that as-prepared CuO cross-rectangular architectures built by thin nanosheets may have more active surface sites for catalytic reaction.

EXPERIMENTAL

1. Synthesis

In a typical experimental procedure, 1 mmol $Cu(CH_3COO)_2 \cdot H_2O$, 6 mmol $NH_3 \cdot H_2O$ and 3 mmol NaOH were added into a 100 mL conical flask containing 60 mL deionized water under stirring. The obtained reaction mixture was transferred into a MAS-II microwave apparatus (power 500 W), and then irradiated for 20 min under

†To whom correspondence should be addressed.
E-mail: hmhu@ustc.edu, chdeng@hfuu.edu.cn

stirring with the rotation speed of 500 r/min at the refluxing temperature of 80 °C. After cooling to room temperature, the obtained black products were washed with anhydrous ethanol and deionized water for several times, and then finally dried in a vacuum at 60 °C for 6 h.

2. Instrument and Characterization

Microwave-heating was performed on a MAS-II microwave synthesis/extraction reaction workstation (work frequency 2.45 GHz, power adjustable range 0-1,000 W, Shanghai Sineo Microwave Chemistry Technology Co., Shanghai, China). The phase structure of the as-prepared products was measured on a Theta/Theta rotating anode X-ray diffractometer (XRD, Rigaku TTR-III, 18 kW, λ=1.5418 Å) using standard Cu Kα radiation. Field-emission scanning electron microscope (FESEM) images of the sample were taken on a field-emission microscope (FEI Sirion 200, 15 kV). Transmission electron microscope (TEM) and high-resolution transmission electron microscope (HRTEM) images of the samples were performed on an H-7650 transmission electron microscope and a high-resolution transmission electron microscope (JEOL JEM-2010). UV-vis absorption spectrum was recorded on a UV-vis spectrophotometer (PerkinElmer Lambda 950). Thermo-gravimetric (TG) and differential scanning calorimetry (DSC) curves were obtained by thermoanalysis (NETZSCH STA 409 PC/PG).

3. Photocatalytic Performance

The prepared CuO cross-rectangular architectures were applied as photocatalyst for the degradation of Rhodamine B (RhB) dye in the presence of hydrogen peroxide (H_2O_2). The irradiation was performed by using a 500 W tungsten lamp as a source of visible light. In the experiment, 100 mg CuO catalyst was added into 60 mL RhB solution (10 mg/L) under magnetic stirring, and the obtained suspension was magnetically stirred at dark for 30 min to establish an adsorption/desorption equilibrium state. Afterwards, 1.0 mL H_2O_2 (30%, w/w) was dropped into the above suspension, and then the suspension was irradiated by tungsten lamp with constant stirring; the reaction temperature was kept constant by using a self-made cooling water recirculation system. At certain time intervals, specific amount of the solution was taken out and centrifuged to remove the catalyst. The concentration change of RhB was immediately detected on a UV-vis spectrophotometer (UV-5500PC).

4. Catalytic Thermal-decomposition of NH_4ClO_4

Thermo-gravimetric (TG) and differential scanning calorimetry (DSC) were used to evaluate catalytic activity on thermal-decomposition of NH_4ClO_4. The prepared CuO cross-rectangular architectures mixed with NH_4ClO_4 by carefully grinding in mass ratio of 4 : 96. The measurement was in an N_2 atmosphere heated from room temperature to 650 °C at a heating rate of 10 °C/min.

RESULTS AND DISCUSSION

1. XRD and EDX Analysis

XRD pattern of the as-synthesized sample is shown in Fig. 1(a). All diffraction peaks could be easily assigned to monoclinic CuO (PDF, No. 05-0661, a=0.4684 nm, b=0.3425 nm, c=0.5129 nm). No characteristic peaks from impurities, such as $Cu(OH)_2$ or Cu_2O, were detected. The strong and sharp reflection peaks suggest that the products are highly crystalline. Fig. 1(b) is the relevant EDX spectrum of the sample, which indicates only the existence of Cu and O elements in the prepared products (the peak of silicon comes from the substrate).

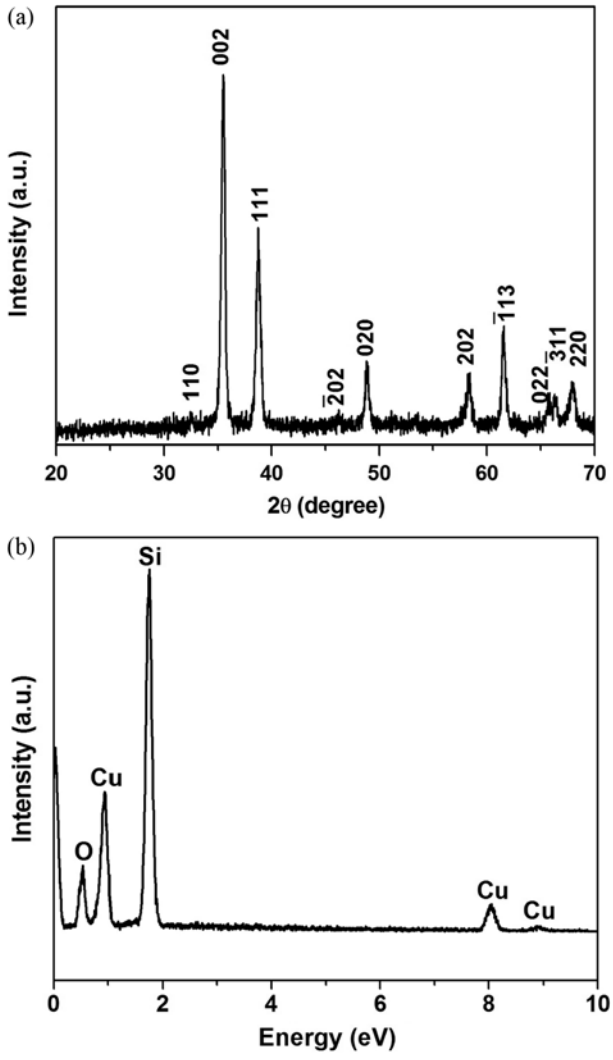

Fig. 1. XRD pattern (a) and EDX result (b) of the CuO sample.

2. Morphology and Structure Analysis

The morphology of the CuO product is studied by field emission scanning electron microscopy (FESEM), as displayed in Fig. 2. One can see that large quantities of uniform perpendicularly cross-rectangular architectures are present in the products. By careful analysis, we can deduce that most of CuO microstructures are mainly assembled by two rectangle-shaped nanosheets with different sizes, which is perpendicularly intersected through the center. Exactly speaking, the big nanosheet is the primary body, and the small one is a secondary generation branch off the central section of the primary body perpendicularly (inset of Fig. 2(a) and (b)). The widths and lengths of the primary CuO rectangular nanosheets are calculated to be 400-700 nm and 2-3 μm, respectively. The thicknesses of nanosheets are estimated to be 20-60 nm. Additionally, two or more small secondary nanosheets growing on the surface of primary body are also occasionally found in the products (indicated by the black circle in Fig. 2(a)).

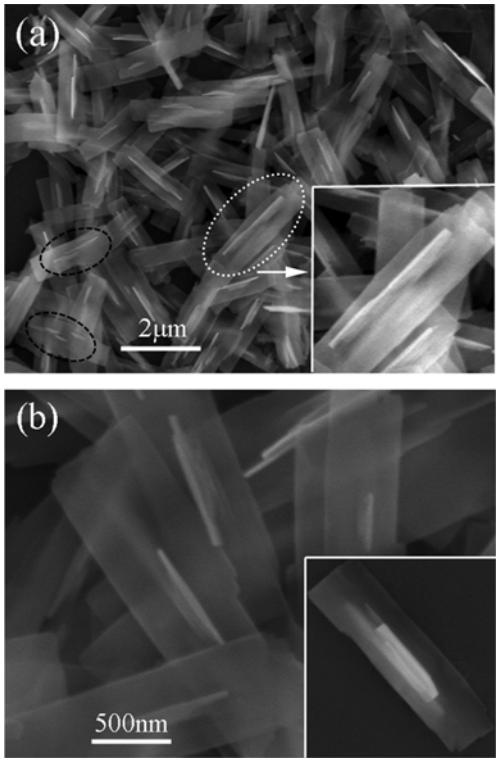

Fig. 2. FESEM images of the prepared perpendicularly cross-rectangular CuO architectures.

The detailed structural characterization of CuO sample was further investigated by TEM and HRTEM microscopy, as shown in Fig. 3. From Fig. 3(a), four edges of a piece of nanosheet are distinctly observed with respect to an individual CuO cross-rectangular nanocrystal, agreeing with FESEM results. In Fig. 3(b) the thickness of the center in the same nanosheet is obviously larger than that of the edge by measurement. It may be suggested that the secondary nucleation and growth easily tend to take place on the central section of primary nanosheet, and would lead to the formation of CuO cross-rectangular architecture. Fig. 3(c) shows a well-developed cross-rectangular architecture, and the width and length of primary nanosheet is about 680 nm and 2.60 μm. The corresponding SAED pattern of the primary nanosheet (inset of Fig. 3(c)) can be indexed to the [001] zone axis of monoclinic CuO, indicating that the nanosheet is single crystal nature with a growth direction of [010]. A typical HRTEM image of the edge of primary nanosheet is shown in Fig. 3(d), and the average distance between the adjacent lattice planes is 0.275 nm, corresponding to the (110) plane, further confirming its growth along [010] direction.

3. Influencing Factors and Growth Mechanism

The effects of NaOH and $NH_3 \cdot H_2O$ on the shapes and sizes of CuO nanocrystallites have been investigated, as illustrated in Fig. 4. It is found that the introduction of NaOH is indispensable for the growth of two-dimensional (2D) CuO nanostructures. If no NaOH is added into the reaction system while keeping other parameters constant, the products are mulberry-shaped CuO nanograins with long diameters of 100-200 nm and short diameters of 50-100 nm (Fig. 4(a)). It can be seen that an individual CuO nanomulbery is assembled by numerous tiny nanoparticles. If the dosage of NaOH is increased to 5 mmol, most of the CuO products are perpendicularly cross-rectangular architectures, but a handful of CuO products have evolved into corn-leaf-like nanosheets with shuttle-

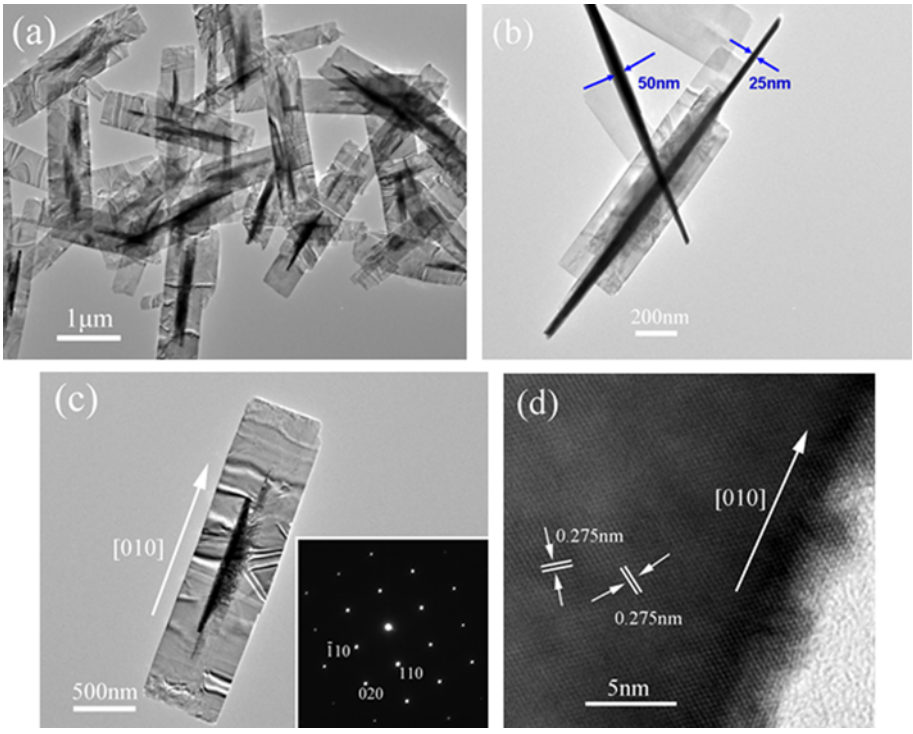

Fig. 3. TEM and HRTEM images of the perpendicularly cross-rectangular CuO architectures.

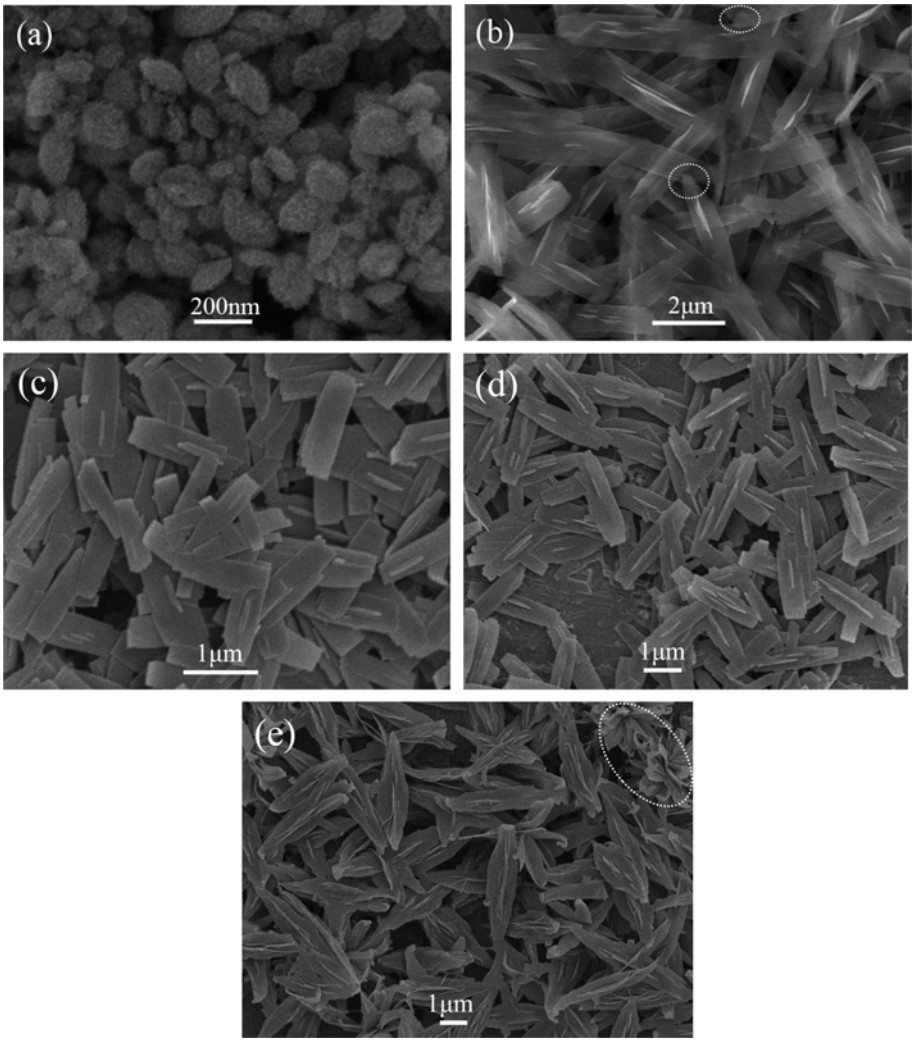

Fig. 4. FESEM images (a)-(b) of the CuO products obtained by only changing the dosage of NaOH: (a) 0 mmol NaOH, (b) 5 mmol NaOH, FESEM images (c)-(e) of the CuO products obtained by only changing the dosage of $NH_3 \cdot H_2O$: (c) 0 mmol $NH_3 \cdot H_2O$, (d) 3 mmol $NH_3 \cdot H_2O$, (e) 10 mmol $NH_3 \cdot H_2O$.

shaped end edge (Fig. 4(b)). In addition, an interesting phenomenon is that the introduction of $NH_3 \cdot H_2O$ is essential for the second nucleation and growth on the pre-generated primary nanosheet. Fig. 4(c)-(d) and (e) show the morphologies of CuO products synthesized by changing the amount of $NH_3 \cdot H_2O$ maintaining other conditions unchanged. If no $NH_3 \cdot H_2O$ is used, the synthesized CuO products are mainly single rectangular nanosheets; the growth of second generation is only occasionally found (Fig. 4(c)). When 3 mmol $NH_3 \cdot H_2O$ is added, large quantities of CuO cross-rectangular architectures are produced due to the second nucleation and growth on the primary rectangular nanosheets (Fig. 4(d)). Fig. 4(e) shows the morphologies of CuO products obtained with the amount of 10 mmol $NH_3 \cdot H_2O$, which suggests that excessive second nucleation and growth probably will take place and lead to the formation of nanosheet-aggregated leaf-like and flower-like CuO crystallites (indicated by the white circle in Fig. 4(e)).

To investigate the formation process of CuO cross-rectangular architecture, time-dependent experiments were performed, maintaining other conditions unchanged. When the microwave irradiating time is reduced to 5 min, a good deal of thin rectangular CuO nanosheets and a handful of underdeveloped cross-rectangular architectures are observed in the products (Fig. 5(a)). Fig. 5(b) shows the morphology of CuO products when the reaction time is 10 min, indicating that abundant CuO cross-rectangular architectures have been produced.

On the base of influencing factors and time-dependent experimental results, a possible formation mechanism of the perpendicularly cross-rectangular CuO architectures is described as follows, as shown in Fig. 6. In the initial stage of the reaction, Cu^{2+} ions would coordinate with NH_3 and OH^- to produce $[Cu(NH_3)_4]^{2+}$ and $[Cu(OH)_4]^{2-}$ complexes Eq. (1)-(2). By the dehydration of preformed $[Cu(OH)_4]^{2-}$ under microwave irradiation Eq. (3), CuO nuclei come into being and rapidly grow into nanoparticles. Then, CuO rectangular nanosheets are formed with further 2D growth of CuO nanoparticles along [010] direction. Finally, secondary nucleation and growth would occur at high-energy central site of larger lying nanosheets under the attack of $[Cu(NH_3)_4]^{2+}$ in the solution. Thus, perpendicularly cross-rectangular CuO architectures are success-

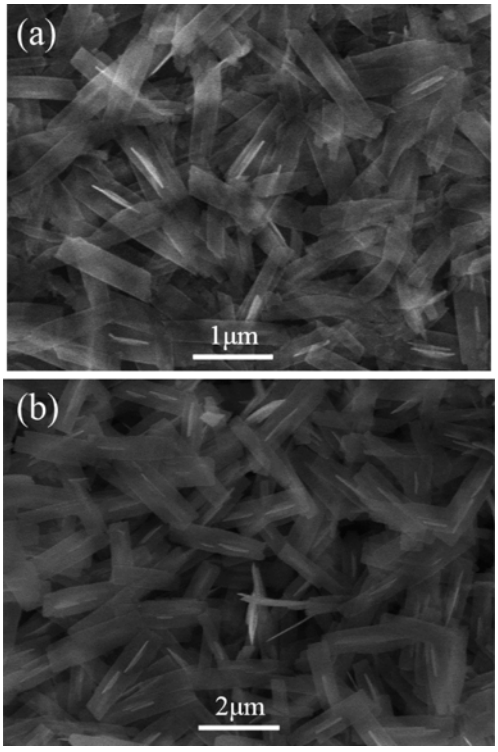

Fig. 5. FESEM images of CuO products obtained at different growth stages: (a) 5 min, (b) 10 min.

fully acquired.

$$Cu^{2+}+4NH_3 \leftrightarrow [Cu(NH_3)_4]^{2+} \quad (1)$$

$$Cu^{2+}+4OH^- \rightarrow [Cu(OH)_4]^{2-} \quad (2)$$

$$[Cu(OH)_4]^{2-} \rightarrow CuO+H_2O+2OH^- \quad (3)$$

4. Photocatalytic Performance

Fig. 7(a) shows the UV-visible absorption spectrum of as-prepared CuO cross-rectangular architectures. One can see that there is a wide absorption ranging from 250 to 800 nm with the absorption peak mainly locating at 400-500 nm. It is suggested that the prepared CuO architectures may have photocatalytic activity on the degradation of organic dyes under visible light.

The photocatalytic activities of the prepared CuO cross-rectangular architectures were evaluated by the oxidation and decoloration of a model organic pollutant Rhodamine B with the assistance of H_2O_2 under tungsten lamp irradiation. Fig. 7(b) presents the time-dependent absorption spectra of RhB aqueous solution in the presence of as-prepared CuO and H_2O_2, indicating that the maximum absorption peak at 554 nm decreases gradually with the extension of illumination time. No new absorption bands appear in either the ultraviolet or visible region, demonstrating the mineralization of RhB on the as-prepared CuO catalyst. About 99% of the RhB was completely decomposed in 120 min. Fig. 7(c) shows the degradation rate (C_t/C_0) at different intervals under different conditions, where C_0 is the initial concentration of RhB and C_t is the concentration of RhB at different illumination time. Comparison experiments were performed to investigate the mechanism of photocatalytic degradation in the present system. For the blank experiment in the absence of CuO and H_2O_2, direct photolysis of RhB could almost be neglected. Only in the presence of CuO was about 5% RhB decomposed in 1 h, possibly due to the fast recombination of photogenerated electron-hole pairs in CuO crystals. Only in the presence of H_2O_2 was the degradation rate 15% in 1 h. It is suggested that H_2O_2 may to some extent combine with photons and generate ·OH radicals, which can oxide RhB molecules. However, the degradation rate of aqueous RhB over as-prepared CuO can reach 97% within 1h in the presence of H_2O_2. For comparison, the degradation process of RhB over commercial CuO was also detected under the same conditions with as-prepared CuO; only about 39% RhB was decomposed in 1 h. The kinetics of RhB degradation was quantitatively studied by applying the pseudo-first-order model [27,28]: $\ln(C_0/C_t)=k\times t$, where C_0 is the initial concentration of dye, C_t is the dye concentration in the solution, t is reaction time, and k is the apparent first-order rate constant. Fig. 7(d) shows the linear plot of $\ln(C_0/C_t)$ versus photocatalytic reaction time t. The rate constant of RhB degradation over as-prepared CuO cross-rectangular architectures is estimated to be 0.05564 min^{-1}, obviously greater than that over the commercial CuO (0.00778 min^{-1}).

Based on the experimental results, the possible reaction process is proposed as follows. First, under the irradiation of tungsten lamp, photogenerated electron-hole pairs are simultaneously generated at conduct band (e^-_{CB}) and valence band (h^+_{VB}) in CuO crystal Eq. (4). Then, as an excellent electron trapping agent, H_2O_2 can com-

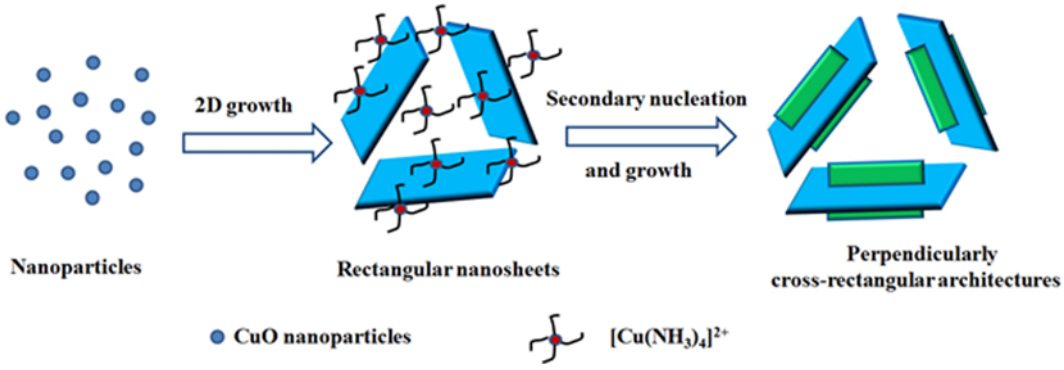

Fig. 6. Schematic illustration of the formation process of the perpendicularly cross-rectangular CuO architectures.

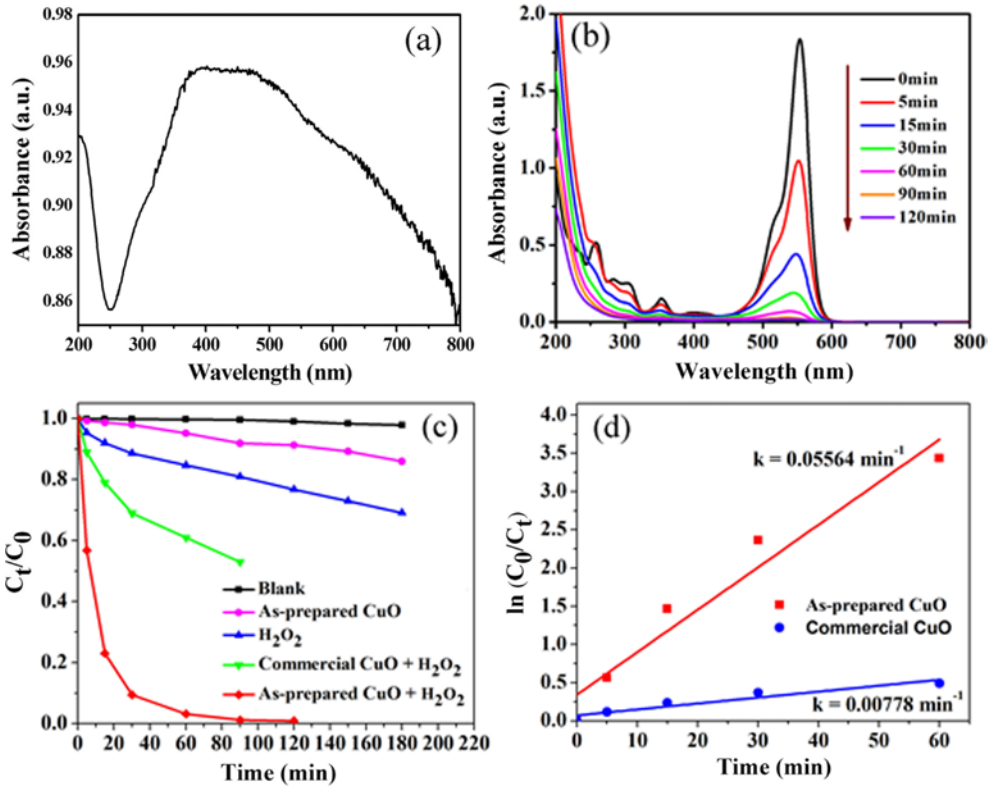

Fig. 7. (a) UV-visible absorption spectrum of as-prepared CuO cross-rectangular architectures, (b) time-dependent absorption spectra of RhB aqueous solutions in the presence of CuO and H_2O_2 under visible-light irradiation, (c) degradation rate of RhB at different intervals under different conditions, (d) the first-order kinetic plots for the photodegradation reaction of RhB.

bine with photogenerated electrons (e^-_{CB}) and produce ·OH radical Eq. (5) [29]. And at the same time, the recombination rate of the photogenerated electron-hole pairs is largely decreased. Finally, h^+_{VB} and ·OH can effectively oxidize and decompose the RhB molecules in the water Eq. (6).

$$CuO+h \rightarrow h^+_{VB}+e^-_{CB} \quad (4)$$

$$H_2O_2+e_{CB} \rightarrow \cdot OH+OH^- \quad (5)$$

$$h^+_{VB}, \cdot OH+RhB \rightarrow CO_2+H_2O \quad (6)$$

5. Catalytic Thermal-decomposition of NH_4ClO_4

Ammonium perchlorate (NH_4ClO_4, AP), an important inorganic energetic compound, has been intensively studied due to its widespread applications in explosives, pyrotechnics and solid rocket propellants [30]. As a potential effective and inexpensive catalyst, CuO micro/nanostructures have been extensively studied on the thermal decomposition of AP [31-37]. The catalytic property of the as-prepared CuO cross-rectangular architectures for the decomposition of AP was evaluated using the reported simultaneous thermal analysis system, as shown in Fig. 8(a). An endothermic peak located at 246 °C is assigned to the reversible crystallographic transition of AP from low-temperature orthorhombic to cubic structure with no associated weight loss [38]. Two exothermic peaks at 314 and 335 °C were observed, which are attributed to the low tem-

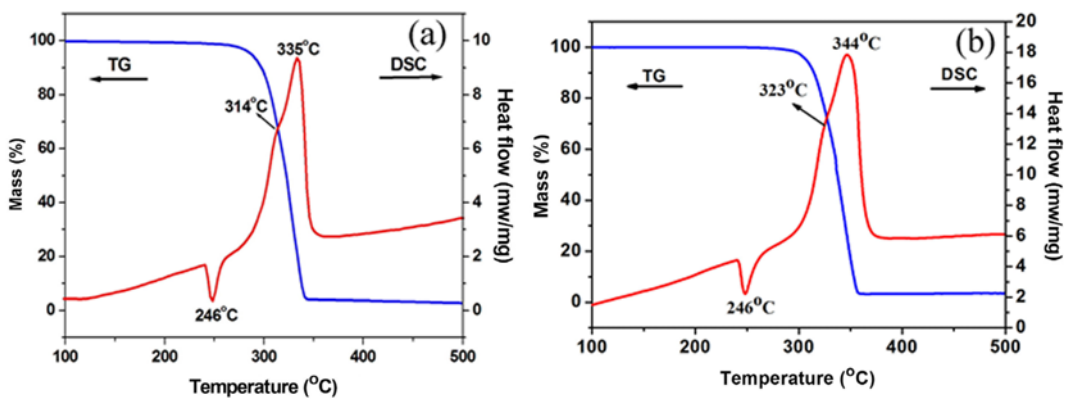

Fig. 8. TG-DSC curves of the mixture of (a) as-prepared CuO and NH_4ClO_4 and (b) commercial CuO and NH_4ClO_4.

perature decomposition (LTD) and high temperature decomposition (HTD) of AP. In Fig. 8, the two decomposition steps almost blend into one process, which is similar to the reported CuO hollow spheres [33]. The decomposition temperature of AP in the mixture of as-prepared CuO and AP system is largely lower than that of pure AP (LTD 347 °C, HTD 425 °C) [33]. The catalytic activity of as-prepared CuO cross-rectangular architectures on the thermal decomposition of AP is almost similar to the peanut-shaped CuO hollow architectures [39]. For comparison, the catalytic property of commercial CuO for the decomposition of AP was also performed under the same conditions, as shown in Fig. 8(b). A low temperature peak at 323 °C and a high temperature peak at 344 °C are detected, which are slightly larger than that of as-prepared CuO. The experimental results also demonstrated the good catalytic activity of the as-prepared CuO cross-rectangular architectures for the thermal decomposition of AP.

CONCLUSIONS

Perpendicularly cross-rectangular CuO architectures composed of nanosheets have been controllably synthesized by a convenient microwave-assisted chemical approach using $Cu(CH_3COO)_2 \cdot H_2O$, $NH_3 \cdot H_2O$ and NaOH as reactants in the solution. HRTEM and ED results both demonstrate that the growth orientation of an individual nanosheet is [010]. The formation mechanism of perpendicularly cross-rectangular CuO architectures was discussed based on the assembly of CuO nanosheets. The prepared CuO cross-rectangular architectures showed excellent photocatalytic activity for degrading Rhodamine B (RhB), and had effective catalytic activity on the thermal decomposition of ammonium perchlorate (NH_4ClO_4).

ACKNOWLEDGEMENTS

This work was supported by the Natural Science Foundation of Anhui Educational Committee (KJ2014ZD08), the Fifth Science and Technology Foundation of Outstanding Youth of Anhui Province (1308085JGD06, 10040606Y25) and the National Natural Science Foundation of China (20501002).

REFERENCES

1. H. Q. Yan, R. R. He, J. Pham and P. D. Yang, *Adv. Mater.*, **15**, 402 (2003).
2. C. Z. Yuan, X. G. Zhang, L. H. Su and L. F. Shen, *J. Mater. Chem.*, **19**, 5772 (2009).
3. H. Jiang, T. Zhao, C. Y. Yan, J. Ma and C. Z. Li, *Nanoscale*, **2**, 2195 (2010).
4. X. L. Hu, J. C. Yu, J. M. Gong, Q. Li and G. S. Li, *Adv. Mater.*, **19**, 2324 (2007).
5. X. W. Lou, D. Deng, J. Y. Lee and L. A. Archer, *J. Mater. Chem.*, **18**, 4397 (2008).
6. X. Wang, C. G. Hu, H. Liu, G. J. Du, X. S. He and Y. Xi, *Sens. Actuat. B-Chem.*, **144**, 220 (2010).
7. U. R. Pillai and S. Deevi, *Appl. Catal. B- Environ.*, **64**, 146 (2006).
8. R. V. Kumar, Y. Diamant and A. Gedanken, *Chem. Mater.*, **12**, 2301 (2000).
9. J. H. Schon, M. Dorget, F. C. Beuran, X. Z. Zu, E. Arushanov, C. D. Cavellin and M. Lagues, *Nature*, **414**, 434 (2001).
10. X. P. Gao, J. L. Bao, G. L. Pan, H. Y. Zhu, P. X. Huang, F. Wu and D. Y. Song, *J. Phys. Chem. B*, **108**, 5547 (2004).
11. Y. W. Zhu, T. Yu, F. C. Cheong, X. J. Xu, C. T. Lim, V. B. C. Tan, J. T. L. Thong and C. H. Sow, *Nanotechnology*, **16**, 88 (2005).
12. F. Bakhtiari and E. Darezereshki, *Mater. Lett.*, **65**, 171 (2011).
13. S. Sonia, N. D. Jayram, P. S. Kumar, D. Mangalaraj, N. Ponpandian and C. Viswanathan, *Superlattices Microstruct.*, **66**, 1 (2014).
14. W. Z. Wang, Y. Zhuang and L. Li, *Mater. Lett.*, **62**, 1724 (2008).
15. X. J. Zhang, G. F. Wang, X. W. Liu and H. Q. Wu, *Mater. Chem. Phys.*, **112**, 726 (2008).
16. X. Q. Wang, G. C. Xi, S. L. Xiong, Y. K. Liu, B. J. Xi, W. C. Yu and Y. T. Qian, *Cryst. Growth Des.*, **7**, 930 (2007).
17. C. H. Deng, H. M. Hu, X. Q. Ge, C. L. Han and B. H. Yang, *J. Nanosci. Nanotechnol.*, **12**, 3150 (2012).
18. M. R. Kim, S. J. Kim and D. J. Jang, *Cryst. Growth Des.*, **10**, 257 (2010).
19. S. Krishnan, A. S. M. A. Haseeb and M. R. Johan, *J. Nanopart. Res.*, **15**, 1410 (2013).
20. Y. Y. Hu, X. T. Huang, K. Wang, J. P. Liu, J. Jiang, R. M. Ding, X. X. Ji and X. Li, *J. Solid State Chem.*, **183**, 662 (2010).
21. G. F. Zou, H. Li, D. W. Zhang, K. Xiong, C. Dong and Y. T. Qian, *J. Phys. Chem. B*, **110**, 1632 (2006).
22. Y. L. Yu and J. Y. Zhang, *Mater. Lett.*, **63**, 1840 (2009).
23. G. Chen, H. F. Zhou, W. Ma, D. Zhang, G. Z. Qiu and X. H. Liu, *Solid State Sci.*, **13**, 2137 (2011).
24. J. Y. Li, S. L. Xiong, B. J. Xi, X. G. Li and Y. T. Qian, *Cryst. Growth Des.*, **9**, 4108 (2009).
25. W. X. Zhang, M. Li, Q. Wang, G. D. Chen, M. Kong and Z. H. Yang, *Adv. Funct. Mater.*, **21**, 3516 (2011).
26. H. X. Shi, Y. X. Zhao, N. Li, K. Wang, X. Hua, M. D. Chen and F. Teng, *Catal. Commun.*, **47**, 7 (2014).
27. Z. H. Ai, W. K. Ho, S. C. Lee and L. Z. Zhang, *Environ. Sci. Technol.*, **43**, 4143 (2009).
28. C. H. Deng and X. B. Tian, *Mater. Res. Bull.*, **48**, 4344 (2009).
29. S. Zaman, A. Zainelabdin, G. Amin, O. Nur and M. Willander, *J. Phys. Chem. Solids*, **73**, 1320 (2012).
30. P. W. M. Jacobs and H. M. Whitehead, *Chem. Rev.*, **69**, 551 (1969).
31. Y. Y. Xu, D. R. Chen, X. L. Jiao and K. Y. Xue, *Mater. Res. Bull.*, **42**, 1723 (2007).
32. P. R. Patil, V. N. Krishnamurthy and S. S. Joshi, *Propell. Explos. Pyrot.*, **33**, 266 (2008).
33. S. Y. Yang, C. F. Wang, L. Chen and S. Chen, *Mater. Chem. Phys.*, **120**, 296 (2010).
34. L. J. Chen, L. P. Li and G. S. Li, *J. Alloy. Comp.*, **464**, 532 (2008).
35. C. Yang, F. Xiao, J. D. Wang and X. T. Su, *J. Colloid Interface Sci.*, **435**, 34 (2014).
36. E. Alizadeh-Gheshlaghi, B. Shaabani, A. Khodayari, Y. Azizian-Kalandaragh and R. Rahimi, *Powder Technol.*, **217**, 330 (2012).
37. C. Yang, J. D. Wang, F. Xiao and X. T. Su, *Powder Technol.*, **264**, 36 (2014).
38. V. V. Boldyrev, *Thermochim. Acta*, **443**, 1 (2006).
39. J. Z. Yin, Z. H. Sheng, W. G. Zhang, Y. Zhang, H. Zhong, R. Q. Li, Z. J. Jiang and X. F. Wang, *Mater. Lett.*, **131**, 317 (2014).